Classification:

Biological Science – Environmental Sciences

Title:

Reducing uncertainties in decadal variability of the global carbon budget with multiple data sets

Wei Li[a,1], Philippe Ciais[a], Yilong Wang[a], Shushi Peng[a], Gregoire Broquet[a], Ashley P. Ballantyne[b], Josep G. Canadell[c], Leila A. Cooper[b], Pierre Friedlingstein[d], Corinne Le Quéré[e], Ranga B. Myneni[f], Glen Peters[g], Shilong Piao[h], Julia Pongratz[i]

Authors from A.P.B. onward are in the alphabetical order of last names.

[a]Laboratoire des Sciences du Climat et de l'Environnement, LSCE/IPSL, CEA-CNRS-UVSQ, Université Paris-Saclay, F-91191 Gif-sur-Yvette, France

[b]Department of Ecosystem and Conservation Science, University of Montana, Missoula, MT, USA

[c]Global Carbon Project, CSIRO Oceans and Atmosphere, GPO Box 3023, Canberra, ACT 2601, Australia

[d]College of Engineering, Mathematics and Physical Sciences, University of Exeter, Exeter EX4 4QF, UK

[e]Tyndall Centre for Climate Change Research, University of East Anglia, Norwich Research Park, Norwich NR4 7TJ, UK

[f]Department of Earth and Environment, Boston University, Boston, MA 02215, USA

[g]Center for International Climate and Environmental Research – Oslo (CICERO), Oslo, Norway

[h]Department of Ecology, College of Urban and Environmental Sciences, Peking University, Beijing 100871, China

[i]Max Planck Institute for Meteorology, Hamburg, Germany

[1]Corresponding author phone: 0033-6-58276925; email: wei.li@lsce.ipsl.fr

Keywords:

global carbon budget; decadal variations; Bayesian fusion

Abstract

Conventional calculations of the global carbon budget infer the land sink as a residual between emissions, atmospheric accumulation and the ocean sink. Thus, the land sink accumulates the errors from the other flux terms and bears the largest uncertainty. Here, we present a Bayesian fusion approach that combines multiple observations in different carbon reservoirs to optimize the land (B) and ocean (O) carbon sinks, land-use change emissions (L), and indirectly fossil fuel emissions (F) from 1980 to 2014. Compared to the conventional approach, Bayesian optimization decreases the uncertainties in B by 41% and in O by 46%. The L uncertainty decreases by 47% whereas F uncertainty is marginally improved through the knowledge of natural fluxes. Both ocean and net land uptake (B+L) rates have positive trends of 29 ± 8 and 37 ± 17 Tg C yr^{-2} since 1980, respectively. Our Bayesian fusion of multiple observations reduces uncertainties thereby allowing us to isolate important variability in global carbon cycle processes.

Significance Statement

The conventional approach of calculating the global carbon budget makes the land sink the most uncertain of all budget terms. This is because rather than being constrained by observations it is inferred as a residual in the budget equation. Here, we overcome this limitation by performing a Bayesian fusion of different available observation-based estimates of decadal carbon fluxes. This approach reduces the uncertainty in the land sink by 41% and in the ocean sink by 46%. These results are significant because they give unprecedented confidence in the role of the increasing land sink in regulating atmospheric CO_2, and shed light on the past decadal trend.

\body

The land and ocean carbon sinks provide a vital climate mitigation 'service' by absorbing on average about 55% of anthropogenic CO_2 emissions from fossil fuel combustion and land-use change. Research has focused on understanding the relationships between year-to-year variability in carbon sinks and climate (1, 2), as well as the long term trend over the full instrumental period of CO_2 monitoring at the Mauna Loa station (3). Quasi-decadal variations of emissions and sinks have received comparatively less attention. Yet, significant climate variation occurs at this specific time scale (4). Since 1980, the variable occurrence of different ENSO events, two large volcanic eruptions (El Chichón and Pinatubo) and the recent slow-down of land surface warming have modulated the strength of carbon sinks. There are also decadal-scale changes in the rate at which human activities perturb the natural carbon cycle, in particular the recent acceleration of fossil fuel and cement emissions in the 2000s (5) and the slow-down in global land-use change emissions (LUC) in the mid-2000s, which appears to be partly driven by reduced deforestation in Brazil (6).

Here, we provide a data-driven assessment of global CO_2 emissions and sinks at 5-year intervals for the period of 1980-2014. We use a new Bayesian fusion approach whereby different data-streams of ocean and land uptake, LUC emissions, are optimally combined, and their uncertainty reduced from prior knowledge. This approach estimates the land sink constrained by data, which is a major improvement over the "conventional" method for calculating the global carbon budget by Ciais et al. (7) and Le Quéré et al. (8), hereafter LQ15, where the unknown land sink was determined as a residual from the other components (emissions, atmospheric increase, ocean uptake). Most of the data-streams used in this analysis start in 1980, and about half of them give decadal mean values of natural sinks and thus do not allow us to tackle the reconstruction of interannual variability. Our choice of applying a Bayesian fusion approach to optimize 5-year

average component fluxes of the global carbon budget is therefore a compromise that maximizes the use of available observations of decadal average fluxes.

The principle of the Bayesian fusion approach is to combine an *a priori* imperfect knowledge of fluxes with observations and their uncertainties to infer optimized estimates of fluxes. Here, we define *a priori* values of terms in the global carbon budget that are not from observations. Specifically, we set prior fossil fuel and cement emissions (F) from inventories and the simulated land, ocean and land-use change carbon fluxes from process-based models (Table S1). The fluxes in this study are only anthropogenic fluxes, assuming a mean CO_2 growth rate of zero during pre-industrial times. Observational data sets independent from those prior values are applied to constrain land-use change emissions (L), the ocean uptake of anthropogenic CO_2 (O), the land-biosphere sink (B) in ecosystems not affected by land-use change, and the net land flux (B+L) (Table S2). We select the constraining data from peer-reviewed publications and evaluate their reported uncertainties and possible error correlations with each other (see details in Table S2).

Results

In the optimization of the global anthropogenic carbon budget (Fig. 1), the prior value of F and its uncertainty (Table S1) were defined from the mean value and the range of different fossil fuel and cement emission inventories, namely from CDIAC (9), IEA (10), EDGAR (11) and BP (12). These emission inventories are not treated as direct observations of emissions, and there is currently no independent observation to verify F. The prior values of O are from seven ocean biogeochemistry models (8), and the prior values of B are from the nine TRENDY land carbon models (13). These prior values from state-of-the-art models are without direct observational constraints. Some of these models could possibly be tuned using similar observation-based data but which observational data were used for model tuning was not explicitly reported. The prior estimates of L are derived from the difference of simulated land carbon fluxes with and without

LUC in the TRENDY carbon models (13). All fluxes are defined as positive if CO_2 is emitted to the atmosphere by the land or the ocean reservoir. Uncertainties in the prior estimates of 5-yearly O, B and L, are set to the maximum between those reported by LQ15 and the standard deviations across models. All uncertainties here refer to 1-σ Gaussian errors. In this context, the prior uncertainties are 0.5 for O, 0.9 for B, and 0.8 Pg C yr^{-1} for L, thus not smaller than the values of 0.5, 0.8 and 0.5 Pg C yr^{-1} from LQ15. It is important that the prior uncertainties are not too small, so that adding observations can adjust and constrain the sought fluxes.

Several independent data-streams, each with their specific uncertainty and temporal averaging period (Table S2), are combined in the Bayesian optimization with the above prior knowledge. These data-streams are: 1) the atmospheric CO_2 growth rate (CGR) from the NOAA/ESRL atmospheric network (14) which constrains the sum of all fluxes and is determined very accurately from more than 60 monitoring stations; 2) the atmospheric 5-year mean (negative) growth rate of O_2/N_2 in the atmosphere from the Scripps O_2 Program (15) which relates to the combined effect of B+L and F changes, while being insensitive to changes in O (note that O_2/N_2 has a negative trend in the atmosphere); 3) a set of yearly mean estimates of O from observational products based on *in situ* partial pressure of CO_2 (pCO_2) surveys corrected for natural ocean CO_2 outgassing from carbon delivered by rivers (16) and using a neural network approach (17) and a diagnostic mixed-layer approach (18), and a set of decadal-mean estimates of O from inventories of carbon change in the ocean deduced indirectly from chlorofluorocarbons (CFCs) (19) combined with ^{14}C (20), and observed atmospheric mean CO_2 level and oceanic CO_2 and dissolved inorganic carbon observations (21); 4) ten-year mean estimates of B from a global synthesis of changes in forest carbon stocks (22); 5) decadal mean B+L from inventory-based land carbon storage change from the RECCAP publications on regional budgets (Table S3); 6) five-year mean LUC emissions from two independent bookkeeping approaches constrained by observed carbon stocks (23, 24). The uncertainties in each data-stream are either derived directly

129 from the original publications (when reported) or estimated from expert judgments (see details in
130 Table S2). The optimization is performed for seven consecutive 5-year windows between 1980
131 and 2014.

132 In the Bayesian optimization, observations that describe mean fluxes during intervals longer than
133 5 years are still useful to infer 5-yearly fluxes. For example, the mean ocean sink observation for
134 the 1990s (19) constrains the mean 5-yearly O during 1990-1999, while other independent
135 observations (O_2/N_2 and CGR) help to further allocate O values between the periods 1990-1994
136 and 1995-1999. Despite no direct observation of F, this flux is found to be slightly improved in
137 the Bayesian fusion, through knowledge of the other terms, and because the sum of all fluxes is
138 very well constrained from CGR observations. We are aware that some observation-based land
139 sink estimates have systematic errors in the way they are included in the optimization. In
140 particular, the estimate of B from ref. (22) is only for forests and ignores other biomes. However,
141 the RECCAP studies (25–27) and other estimates (22, 28) of the carbon stock change in non-
142 forest biomes suggest that the forest sink alone accounts for most of the global land sink B.

143 The improved global budget of anthropogenic CO_2 is shown in Fig. 2, and all data are given in
144 Table S1. After optimization, the *a posteriori* uncertainty in each flux is reduced. Compared to
145 the conventional method applied by LQ15 and IPCC-AR5 (7), uncertainties in B and O are
146 reduced by 41% and 46% in this study. In the Bayesian data fusion, the land sink is no longer
147 solely inferred as a residual that accumulates uncertainties from all other terms, and it exhibits a
148 large reduction in uncertainty. The uncertainty in L decreases by 47% but the uncertainty in F is
149 marginally improved (by 1%) through the indirect constraints of other terms. In the absence of
150 direct constraint on F, this small reduction in the F uncertainties compared to LQ15 and IPCC-
151 AR5 (7) is also because we use multiple emission inventories (while LQ15 and IPCC-AR5 (7)
152 only used CDIAC (9)) and start at relatively higher prior uncertainties in F (Table S1) than in
153 LQ15. Despite their improved (smaller) uncertainties, the 5-year mean fluxes shown in Table S1

154 do not differ statistically in their mean values from LQ15. This indicates that each flux of the
155 Bayesian carbon budget is fully consistent with LQ15 even though we used an array of data with
156 different measurement methods and with uncertainties estimated in different ways. Specifically,
157 we obtain emissions from fossil fuel burning and cement production that are smaller than LQ15
158 by 0.18±0.19 Pg C yr^{-1} during 1980-2014 (Fig. 2). A downward revision of global F is consistent
159 with the correction of the emissions for China based on evidence of the lower carbon content for
160 coal burned in that country (29). Compared to LQ15, the optimized ocean sink during 2000-2004
161 is larger by 0.22 Pg C yr^{-1} but lower by 0.18±0.10 Pg C yr^{-1} during all the other periods. In the
162 past decade (2005-2014), both ocean sink and land sink from our optimization are smaller than
163 LQ15. The optimized fluxes of L are similar to or lower than those from LQ15. The trend of F for
164 the seven 5-year periods is positive (p = 0.003), with a probability of a positive trend for ocean
165 and net land (B+L) uptake rates of 93%; the trend of B or L individually is not statistically
166 significant (p = 0.23 for both). The increasing rate of ocean and net land uptake are 29±8 and
167 37±17 Tg C yr^{-2} since 1980, respectively. Similar statistically positive trends were also found in
168 the 5-year mean ocean and net land uptake rates between 1980 and 2014 calculated from the
169 yearly budget updated by LQ15 (Fig. S1*A*). Given the robustness of O inferred by our
170 optimization (see also Fig. S2), and in view of the many observations constraining this flux, there
171 is a high confidence that the ocean sink has been increasing over time since 1980. The optimized
172 land sink is less variable between different 5-year periods than in LQ15 (Fig. S1*A*). But the ocean
173 sink is more variable, with a standard deviation of 0.34 Pg C yr^{-1} compared to 0.27 Pg C yr^{-1} by
174 LQ15 (standard deviations across the seven periods analyzed).

175 From 1980 to 2014, the average fractions of F+L emission re-absorbed by the land and ocean
176 carbon reservoirs are 29±5% (mean ±1 σ of inter 5-year variability) and 26±2%, respectively. The
177 ratios of both O and B to F+L emission do not exhibit any significant trends (p > 0.05, Fig. S1*B*).
178 Even with their reduced uncertainty in this study compared to LQ15, the variability of O and B

between 5-year intervals prevents us from assessing the very small trends in their ratios to emissions. Similarly, we found no significant trend in the ratio of O or B to fossil fuel emission (F). The larger variability of the B-to-(F+L) ratios compared to the O-to-(F+L) ones (Fig. S1*B*) suggests that the efficiency of the land sink at absorbing emissions is more variable than that of the ocean sink. For instance, during the period that followed the cooling from the Pinatubo eruption in 1990-1994 (30–32), the B-to-(F+L) ratio increased by 46% above its long-term mean. This ratio was also higher than normal during 2005-2009, possibly due to the absence of El Niño and to the occurrence of a cooler and wetter La Niña event in 2008-2009 manifested by lower than normal CGR (3).

Discussion

In our Bayesian fusion, the CGR constrains the sum of the different fluxes, thus an overestimation of a component flux due to the use of a single published estimate of that flux would result in an underestimation of another flux, leading to negative correlations between uncertainties in the different components of the posterior fluxes. These negative correlations are clear between uncertainties in B and F (ranging from -0.80 to -0.35), in B and O (from -0.60 to -0.30), and in B and L (from -0.53 to -0.24) (Fig. S3). This indicates that although the uncertainties for each flux can be significantly decreased, the remaining (posterior) uncertainties are hard to be decoupled. In comparison, we also calculate the correlations between uncertainties in B and other fluxes by classical error propagation rule from mass balance equation B = CGR – F – O – L. The "conventional" error budget calculation gives a typical uncertainty of 0.76 Pg C yr^{-1} for B. Negative error correlations also exist in that approach between B and F (-0.39), between B and O (-0.79), and between B and L (-0.39). Thus in our study, not only the posterior uncertainties of B (0.42-0.53 Pg C yr^{-1}) are smaller than those calculated by the "conventional" approach, but also the negative error correlation between B and O is smaller, indicating a better

separation between the carbon sinks of B and O. In addition, although the negative correlations between B and F, and between B and L are slightly larger than those calculated by the "conventional" approach, it does not mean our approach has poorer ability to separate these components because we have succeed in significantly decreasing the absolute uncertainties for all the fluxes thus allowing us to draw more definitive conclusions.

The Bayesian fusion of different observational components of the anthropogenic CO_2 budget proposed in this study provides the most robust estimate to date of the strength and evolution of the land sink on 5-year intervals and brings a more robust picture of the current perturbation of the carbon cycle. Future work could apply the same fusion approach to regional carbon budget estimates and to gross CO_2 fluxes of photosynthesis, respiration and fire emissions.

Materials and Methods

Bayesian Estimation System. Each estimate of the 5-year mean carbon fluxes, called hereafter the "control variables" **x**, is based on the update from a prior estimate of these variables $\mathbf{x}^{\mathbf{b}}$, using some observation-based estimates $\mathbf{y}^{\mathbf{o}}$ of the fluxes that are connected to the control variables through the relationships H: $\mathbf{x}\rightarrow\mathbf{y}=H[\mathbf{x}]$. We follow a Bayesian statistical approach for this estimation. Assuming that the distributions of uncertainties in $\mathbf{x}^{\mathbf{b}}$ and $\mathbf{y}^{\mathbf{o}}$ are unbiased and Gaussian, being characterized by the prior and observation uncertainty covariance matrices **B** and **R** respectively, and that H is linear (denoted as a matrix **H**), the statistical estimate of **x**, given $\mathbf{x}^{\mathbf{b}}$ and $\mathbf{y}^{\mathbf{o}}$, is unbiased and Gaussian, and the corresponding optimal estimate $\mathbf{x}^{\mathbf{a}}$ and uncertainty covariance matrix **A** are given (33) as:

$$\mathbf{A}=\left(\mathbf{B}^{-1}+\mathbf{H}^{\mathrm{T}}\mathbf{R}^{-1}\mathbf{H}\right)^{-1} \quad (1)$$

$$\mathbf{x}^{\mathrm{a}}=\mathbf{x}^{\mathrm{b}}+\mathbf{A}\mathbf{H}^{\mathrm{T}}\mathbf{R}^{-1}\left(\mathbf{y}^{0}-\mathbf{H}\mathbf{x}^{\mathrm{b}}\right) \quad (2)$$

where the superscripts T and "-1" denote the transpose and inverse of a matrix, respectively.

In the optimization, we update the estimate of the mean fluxes of fossil fuel and cement emissions (F), ocean sink (O), land sink (B) and land-use change emissions (L) for each 5-year interval from 1980 to 2014 (Fig. 1 and Table S1). The observation vector contains estimates of 5-year mean global value for: the atmospheric growth rates of CO_2 (CGR, in Pg C yr^{-1}), atmospheric growth rates of O_2/N_2 (CGR-O_2, per meg unit), observation-based estimates of ocean sinks, land sinks, land-use change emissions and net land sink (B+L) (the data sources for these components of $\mathbf{y}^{\mathbf{o}}$ are summarized in Fig. 1 and provided in Table S2). **H** is defined for each 5-year interval by:

234 $$\mathbf{x} \rightarrow \mathbf{y^o} = \mathbf{Hx}$$
$$\mathbf{H}:\begin{bmatrix} F \\ O \\ B \\ L \end{bmatrix} \rightarrow \begin{bmatrix} CGR \\ CGR - O_2 \\ O \\ B \\ L \\ B+L \end{bmatrix} = \begin{bmatrix} F+O+B+L \\ \alpha_F F + \alpha_B (B+L) + Z_{O2} \\ O \\ B \\ L \\ B+L \end{bmatrix} \quad (3)$$

235 where α_F, α_B and Z_{O2} are constant coefficients from ref. (15).

236 The prior estimates for the different control variables are built with independent data sets so that
237 there are no correlations between the prior uncertainties in the different control variables. When
238 setting up the observation covariance matrix, the temporal correlations between the uncertainties
239 in different 5-year intervals for CGR and O are estimated using the method in ref. (34). The
240 correlations between the uncertainties in the two data-driven estimates of O (17, 18) are estimated
241 from the series of annual fluxes of the two products by assuming that the correlation in annual
242 fluxes within each 5-year period is an approximation of the 5-year mean flux error correlation.

243 **Data used to derive the Prior statistics of the control variables.** To define the prior estimate of
244 F, individual country data from four emission inventories (CDIAC (9), IEA (10), EDGAR (11)
245 and BP (12)) are grouped into geographic regions as specified by the United Nations Statistics
246 Division (http://unstats.un.org/unsd/methods/m49/m49regin.htm). Cement emissions from
247 EDGAR are added into the IEA and BP data sets that do not include cement emissions.
248 Uncertainties for each country (35) are used to create regional uncertainty distributions for each
249 emission index using a bootstrapping method, with the uncertainties of the highest emitters in
250 each region contributing the most to the uncertainty distributions. This effect is achieved by
251 weighting the sampling probability (P_s) by the relative contribution of each country's emissions
252 (E_C) to the total emissions within the region (E_R):

253 $$P_s = \frac{E_C}{E_R} \quad (4)$$

To constrain the temporal component of the emission errors, ten random samples are drawn from the corresponding regional uncertainty distribution for each country, producing ten random uncertainties for each country. These country-level uncertainties are used to constrain a random error time series covering 1980-2014, which is then run through an algorithm incorporating autocorrelated random noise, such that:

$$\varepsilon_{F(t)} = 0.95 \times \varepsilon_{F(t-1)} + \varepsilon_{(t)} \quad (5)$$

where emission error factors for any given year $\varepsilon_{F(t)}$ are correlated with the emission errors from the previous year $\varepsilon_{F(t-1)}$ by an autoregressive coefficient of 0.95 with $\varepsilon_{(t)}$ as random error. The autocorrelated time series are then multiplied and added to the fossil fuel emissions for each country, and subsequently 500 samples of global fossil fuel emissions are taken for each 5-year bin. The means and standard deviations of each bin for each inventory are calculated from these 500 samples. Additionally, the correlation in global uncertainty is calculated between 5-year bins and inventories to produce an error-covariance matrix. The maximum between the uncertainties calculated above and the standard deviations of the 5-year means across four emission inventories were adopted as the uncertainties in the prior estimate of F.

Prior O values are set from the ocean biogeochemistry model values used in LQ15, which represent state-of-the-art ocean models and are generally consistent with estimates from data-based products (8). Note that LQ15 adjusted their simulated O so as to match ocean observations during the decade of the 1990s and then used these bias-corrected ocean models outside this period (see adjusted values in Table S1). Here, for setting the prior O estimate and uncertainty, we consider simply the spread and the mean of ocean models without any adjustment, because the adjustment performed by LQ15 is already a kind of model data-fusion approach based on the ocean observations used in our study.

277 Prior values of L and B are set from simulations in the TRENDY (v2) model intercomparison
278 project (13). The simulations in TRENDY (v2) are up to 2012, and thus the priors for the period
279 of 2010-2012 were used for the period of 2010-2014. All the prior flux values are summarized in
280 Table S1.

281 **Uncertainty Correlations between Optimized Variables.** The correlations of the uncertainties
282 between optimized variables are shown in Fig. S3. In comparison, we also calculate the
283 correlations between uncertainties in the fluxes when deriving the estimate of B using the
284 classical mass balance equation B = CGR - F - O – L. First, the uncertainties in an estimate of the
285 flux i is calculated using inverse variance method, based on the variances associated with all the
286 estimates of this flux (j=1,2,…,m):

287 $$\sigma_i = \sqrt{\frac{1}{\sum_{j=1}^{m} \frac{1}{\sigma_{i,j}^2}}} \quad (6)$$

288 The resulting uncertainties for CGR, F, O and L are: 0.2, 0.3, 0.6 and 0.3 Pg C yr^{-1}, respectively.
289 Based on a simple error propagation: $\varepsilon_B = \varepsilon_{CGR} - \varepsilon_F - \varepsilon_O - \varepsilon_L$ and the independence of the
290 estimates of CGR, F, O and L, the variance of the uncertainty in B is given by:

291 $$\sigma_B^2 = E(\varepsilon_B^T \varepsilon_B) = \sigma_{CGR}^2 + \sigma_F^2 + \sigma_O^2 + \sigma_L^2 \quad (7)$$

292 where E(.) is the expectation of a variable. The correlation between the uncertainties in B and in
293 another variable, e.g. O in the equation below, is given by:

294 $$r(\varepsilon_B, \varepsilon_O) = \frac{E(\varepsilon_B^T \varepsilon_O)}{\sigma_B \sigma_O} = -\frac{\sigma_O}{\sigma_B} \quad (8)$$

295 **Sensitivity Tests.** Four sets of sensitivity tests were conducted (Fig. S2): (a) using F from
296 different inventory data sets (IEA, EDGAR, CDIAC and BP, respectively) as priors; (b) using
297 different ocean constraining data sets (only data from ref. (17), only data from ref. (18), data from
298 ref. (17) and (18) but without other ocean data, and all ocean data except ref. (19), respectively);

(c) using different tiers of constraining data (Tier 1 only, Tier 1 + Tier 2, and Tier1 + Tier 2 + Tier 3, respectively); and (d) using enlarged prior uncertainties (10^6 Pg C yr^{-1} except F), prior B and O from CMIP5 models (36) instead of TRENDY (v2) models, and a subset of constraining data including CGR, O_2/N_2, L from ref. (24) and O from pCO_2 and inventories (17, 18, 20). The constraining data tiers (Table S2) were defined as: Tier 1, direct carbon observations (e.g. CGR); Tier 2, indirect carbon observations unambiguously related to carbon quantities (e.g. O_2/N_2); Tier 3, direct carbon observations with an empirical (data-driven) model used to obtain global estimates, e.g. the use of geo-statistics to up-scale local data into global values; Tier 4, indirect carbon observations not simply related to global carbon flux quantities.

The ocean sink is rather consistent in all sensitivity tests (Fig. S2), implying it is very robustly constrained in the optimization because of the sufficient number and consistency of constraining observational data (see the O constraining data in Table S2). Small changes in optimized F were found (Fig. S2*A*) in the sensitivity tests using prior F from different data sets, and the land sink is more dependent on the prior F choice. In the sensitivity tests using different ocean constraining data (Fig. S2*B*), all fluxes are generally consistent, and very slight changes for O appear in the tests using ocean data from ref. (17) only and from ref. (18) only during 2000-2004 and 2005-2009. The decadal estimates (19–21) only have small impact on their corresponding periods. The important point for the sensitivity tests using different tiers of constraining data is that there is no inconsistency (i.e. shift in posterior estimate) between the assimilations of different "observation based" tiers although L may change due to lack of individual constrains in Tier 1 and Tier 1 + Tier 2 (Fig. S2*C*). With enlarged prior uncertainties (10^6 Pg C yr^{-1} except F), the mean flux values do not shift in general but the posterior uncertainties increase (Fig. S2*D*). Results are also very consistent by replacing prior B and O from TRENDY v2 models with from CMIP5 models (Fig. S2*D*). The sensitivity test using a subset of constraining data underestimate B and L compared to

the original optimized results (Fig. S2*D*) because the L estimates in ref. (23) (used in the original optimization but not in this sensitivity test) is higher than that in ref. (24) (Table S2).

Trend Test. A Mann-Kendall statistical test was applied as a trend test.

Acknowledgements

This paper builds on an analysis started by the late Michael R. Raupach and is a contribution to the work of the Global Carbon Project to understand and better constrain the human perturbation of the carbon budget. We thank Alessandro Anav for providing the data from CMIP5 and Peter Landschützer and Christian Rödenbeck for sharing their ocean flux data. We are grateful to the scientists from NOAA/ESRL and the Scripps O_2 Program for making the invaluable data from the long-term measurements of CGR and O_2/N_2 available to the community.

W.L. is supported by the European Commission-funded project LUC4C (No. 603542). P.C. and S.Pe. acknowledge support from the European Research Council through Synergy grant ERC-2013-SyG-610028 "IMBALANCE-P". J.G.C. is supported by the Australian Climate Change Science Program, G.P. is supported by the Norwegian Research Council (236296), and J.P. is supported by the German Research Foundation's Emmy Noether Program.

References

1. Wang X, et al. (2014) A two-fold increase of carbon cycle sensitivity to tropical temperature variations. *Nature* 506(7487):212–5.

2. Poulter B, et al. (2014) Contribution of semi-arid ecosystems to interannual variability of the global carbon cycle. *Nature* 509(7502):600–3.

3. Le Quéré C, et al. (2009) Trends in the sources and sinks of carbon dioxide. *Nat Geosci* 2(12):831–836.

4. Ghil M, Vautard R (1991) Interdecadal oscillations and the warming trend in global temperature time series. *Nature* 350(6316):324–327.

5. Raupach MR, et al. (2007) Global and regional drivers of accelerating CO2 emissions. *Proc Natl Acad Sci U S A* 104(24):10288–93.

6. Song X-P, Huang C, Saatchi SS, Hansen MC, Townshend JR (2015) Annual Carbon Emissions from Deforestation in the Amazon Basin between 2000 and 2010. *PLoS One* 10:e0126754.

7. Ciais P, et al. (2013) 2013: Carbon and Other Biogeochemical Cycles. *Clim Chang 2013 Phys Sci Basis Contrib Work Gr I to Fifth Assess Rep Intergov Panel Clim Chang*:465–570.

8. Le Quéré C, et al. (2015) Global carbon budget 2014. *Earth Syst Sci Data*:47–85.

9. Boden TA, Marland G, Andres RJ (2013) Global, regional, and national fossil-fuel CO_2 emissions. *Carbon Dioxide Inf Anal Center, Oak Ridge Natl Lab USA Oak Ridge, TN Dep Energy*. doi:10.3334/CDIAC/00001.

10. International Energy Agency (2013) CO2 Emissions From Fuel Combustion Highlights. *IEA Stat*:158.

11. Olivier JGJ, Janssens-Maenhout G, Peters JAHW (2014) *Trends in global CO2 emissions: 2014 Report* (PBL Netherlands Environmental Assessment Agency Hague).

12. BP (2015) BP Statistical Review of World Energy 2015.

13. Sitch S, et al. (2015) Recent trends and drivers of regional sources and sinks of carbon dioxide. *Biogeosciences* 12(3):653–679.

14. NOAA/ESRL NOAA/ESRL calculation of global means. Available at: http://www.esrl.noaa.gov/gmd/ccgg/about/global_means.html [Accessed August 9, 2015].

15. Keeling RF, Manning a. C (2014) *Studies of Recent Changes in Atmospheric O2 Content* (Elsevier Ltd.). 2nd Ed. doi:10.1016/B978-0-08-095975-7.00420-4.

16. Jacobson AR, Fletcher SEM, Gruber N, Sarmiento JL, Gloor M (2007) A joint atmosphere-ocean inversion for surface fluxes of carbon dioxide: 1. Methods and global-scale fluxes. *Global Biogeochem Cycles* 21(1). doi:10.1029/2005GB002556.

17. Landschützer P, Gruber N, Bakker DCE, Schuster U (2014) Recent variability of the global ocean carbon sink. *Global Biogeochem Cycles* 28(9):927–949.

18. Rödenbeck C, et al. (2014) Interannual sea–air CO_2 flux variability from an observation-driven ocean mixed-layer scheme. *Biogeosciences* 11(17):4599–4613.

19. McNeil BI, Matear RJ, Key RM, Bullister JL, Sarmiento JL (2003) Anthropogenic CO2 uptake by the ocean based on the global chlorofluorocarbon data set. *Science* 299(5604):235–9.

20. Khatiwala S, Primeau F, Hall T (2009) Reconstruction of the history of anthropogenic CO(2) concentrations in the ocean. *Nature* 462(7271):346–9.

21. Steinkamp K, Gruber N (2013) A joint atmosphere-ocean inversion for the estimation of seasonal

carbon sources and sinks. *Global Biogeochem Cycles* 27(3):732–745.

22. Pan Y, et al. (2011) A large and persistent carbon sink in the world's forests. *Science* 333(6045):988–993.

23. Hansis E, Davis SJ, Pongratz J (2015) Relevance of methodological choices for accounting of land use change carbon fluxes. *Global Biogeochem Cycles* 29(8):1230–1246.

24. Houghton R a., et al. (2012) Carbon emissions from land use and land-cover change. *Biogeosciences* 9(12):5125–5142.

25. Piao SL, et al. (2012) The carbon budget of terrestrial ecosystems in East Asia over the last two decades. *Biogeosciences* 9(9):3571–3586.

26. Luyssaert S, et al. (2012) The European land and inland water CO_2, CO, CH_4 and N_2O balance between 2001 and 2005. *Biogeosciences* 9(8):3357–3380.

27. King AW, et al. (2015) North America's net terrestrial CO_2 exchange with the atmosphere 1990–2009. *Biogeosciences* 12(2):399–414.

28. Liu YY, et al. (2015) Recent reversal in loss of global terrestrial biomass. *Nat Clim Chang* 5(5):470–474.

29. Liu Z, et al. (2015) Reduced carbon emission estimates from fossil fuel combustion and cement production in China. *Nature* 524(7565):335–338.

30. Lucht W, et al. (2002) Climatic control of the high-latitude vegetation greening trend and Pinatubo effect. *Science* 296(5573):1687–9.

31. Mercado LM, et al. (2009) Impact of changes in diffuse radiation on the global land carbon sink. *Nature* 458(7241):1014–7.

32. Frölicher TL, Joos F, Raible CC, Sarmiento JL (2013) Atmospheric CO2 response to volcanic eruptions: The role of ENSO, season, and variability. *Global Biogeochem Cycles* 27(1):239–251.

33. Tarantola A (2005) *Inverse Problem Theory and Methods for Model Parameter Estimation* (SIAM).

34. Ballantyne AP, et al. (2015) Audit of the global carbon budget: estimate errors and their impact on uptake uncertainty. *Biogeosciences* 12(8):2565–2584.

35. Andres RJ, Boden TA, Higdon D (2014) A new evaluation of the uncertainty associated with CDIAC estimates of fossil fuel carbon dioxide emission. *Tellus B* 66. doi:10.3402/tellusb.v66.23616.

36. Anav A, et al. (2013) Evaluating the Land and Ocean Components of the Global Carbon Cycle in the CMIP5 Earth System Models. *J Clim* 26(18):6801–6843.

37. Rödenbeck C, et al. (2015) Data-based estimates of the ocean carbon sink variability - First results of the Surface Ocean pCO2 Mapping intercomparison (SOCOM). *Biogeosciences* 12(23):7251–7278.

38. Rödenbeck C, et al. (2013) Global surface-ocean p^{CO_2} and sea–air CO_2 flux variability from an observation-driven ocean mixed-layer scheme. *Ocean Sci* 9(2):193–216.

39. Hurtt GC, et al. (2011) Harmonization of land-use scenarios for the period 1500–2100: 600 years of global gridded annual land-use transitions, wood harvest, and resulting secondary lands. *Clim Change* 109(1–2):117–161.

40. King AW, et al. (2015) North America's net terrestrial CO2 exchange with the atmosphere 1990-2009. *Biogeosciences* 12(2):399–414.

41. Peters GP, Davis SJ, Andrew R (2012) A synthesis of carbon in international trade. *Biogeosciences*

9(8):3247–3276.

42. Hartmann J, Jansen N, Dürr HH, Kempe S, Köhler P (2009) Global CO2-consumption by chemical weathering: What is the contribution of highly active weathering regions? *Glob Planet Change* 69(4):185–194.

43. Dolman AJ, et al. (2012) An estimate of the terrestrial carbon budget of Russia using inventory-based, eddy covariance and inversion methods. *Biogeosciences* 9(12):5323–5340.

44. Lauerwald R, Laruelle GG, Hartmann J, Ciais P, Regnier PAG (2015) Spatial patterns in CO2 evasion from the global river network. *Global Biogeochem Cycles* 29(5):2014GB004941.

45. Gloor M, et al. (2012) The carbon balance of South America: a review of the status, decadal trends and main determinants. *Biogeosciences* 9(12):5407–5430.

46. Valentini R, et al. (2014) A full greenhouse gases budget of Africa: synthesis, uncertainties, and vulnerabilities. *Biogeosciences* 11(2):381–407.

47. Haverd V, et al. (2013) The Australian terrestrial carbon budget. *Biogeosciences* 10(2):851–869.

Figure captions:

Fig. 1. The framework of our optimization. The number of constraining data-streams and the specific data sources are marked on the right. The fluxes that are optimized are 5-year averages of F, O, B and L representing fossil fuel and cement emissions, ocean sink, land sink, and land-use change emissions, respectively. The observations used to constrain these fluxes are the five-year averaged growth rates of CO_2 and O_2/N_2 in the atmosphere, observations of O and B from carbon measurements made in these two reservoirs, and inventory-based estimates of L and the net land sink (B+L). In this framework, the CO_2 growth rate constrains the sum of all the fluxes. The O_2/N_2 growth rate allows us to separate O and B+L and bring some constraint on F as well.

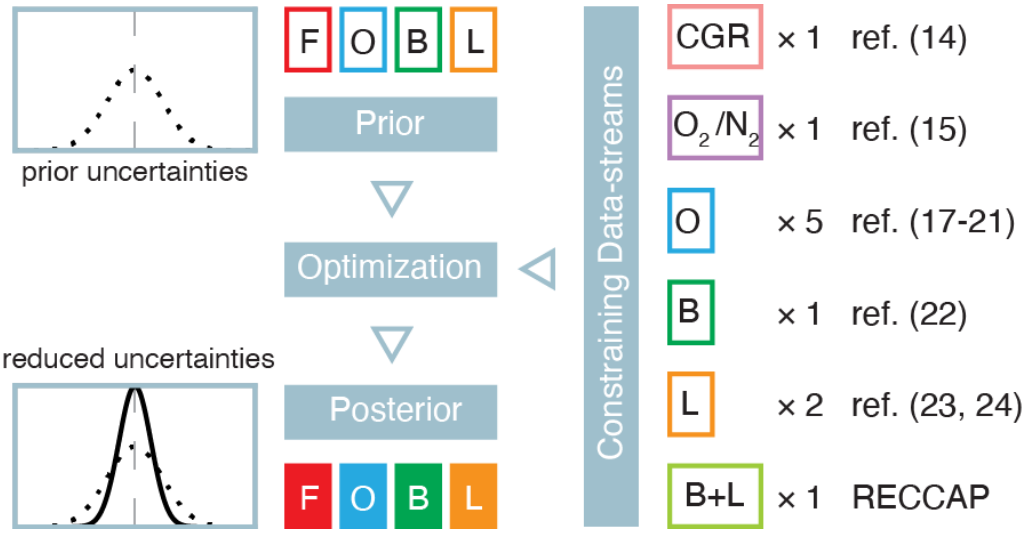

Fig. 2. (*A*) The fossil fuel and cement emissions (F), (*B*) ocean sink (O) and (*C*) net land flux (B+L), and (*D*) land sink (B) and land-use change emissions (L) from prior knowledge, posterior results and LQ15. All the fluxes are 5-year means in each period. The error bars represent the 1-σ uncertainties.

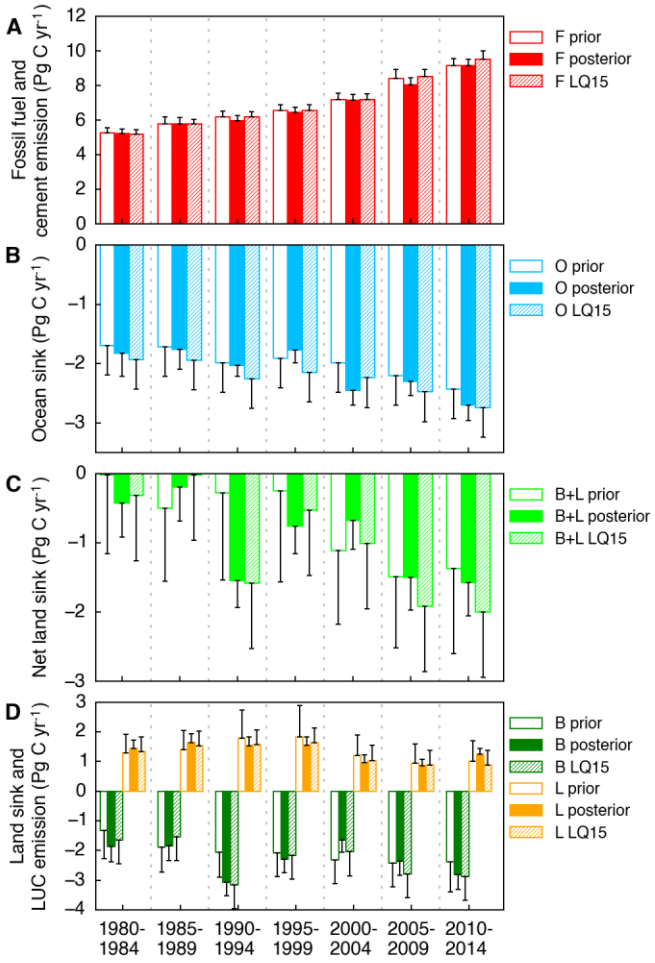

SI Figure captions:

Fig. S1. (*A*) The temporal trend of ocean sink (O), land sink (B), land-use change emissions (L) and net land flux (B+L) from our optimization and LQ15. (*B*) The partitioning of global total emissions (fossil fuel and cement emissions and land-use change emissions, F+L) into atmosphere, ocean (O) and biosphere (B, background shade). The markers are absolute absorbed fractions and uncertainties in ocean (blue squares) and biosphere (green squares).

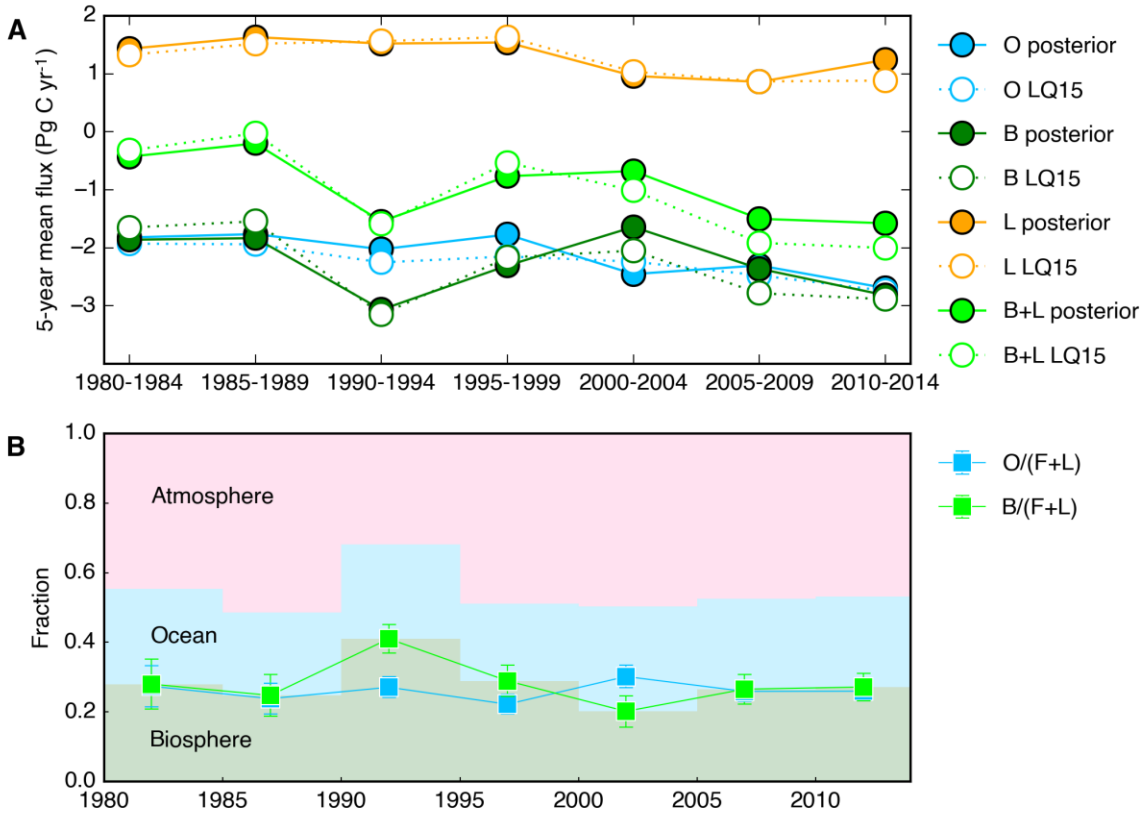

Fig. S2. Sensitivity tests using different data sets. F, O, B, L and B+L indicate fossil fuel and cement emissions, ocean sink, land sink, land use change emissions and net land sink, respectively. (*A*) Using F from different inventory data sets as priors. The bars around each flux in each period from left to right represent the original optimization, double prior uncertainties, prior F from IEA, prior F from EDGAR, prior F from CDIAC and prior F from BP, respectively. (*B*) Using different ocean constraining data sets. The bars from left to right represent the original optimization (all ocean data), only data from ref. (17), only data from ref. (18), data from ref. (17) and (18) but without other ocean data, all ocean data except ref. (19), respectively. (*C*) Using different tiers (Tier number shown in Table S2) of constraining data. The bars from left to right represent the original optimization (all tiers), Tier 1 only, Tier 1 + Tier 2, Tier1 + Tier 2 + Tier 3, respectively. (*D*) The bars from left to right represent the original optimization, enlarging prior uncertainties to 10^6 Pg C yr^{-1} except F, prior B and O from CMIP5, and using a subset of constraining data including CGR, O_2/N_2, L from ref. (24) and O based on pCO_2 and inventories (17, 18, 20).

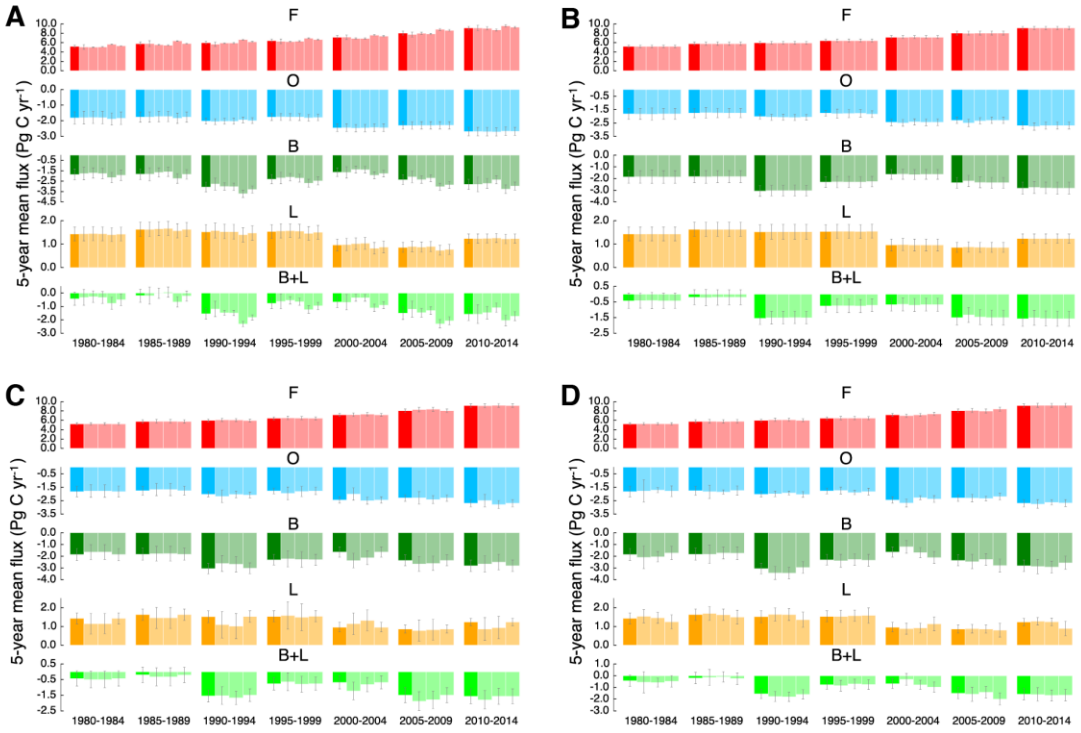

Fig. S3. Correlations between the posterior uncertainties. The subscripts 1 to 7 represent the 5-year periods from 1980-1984 to 2010-2014 in sequence.

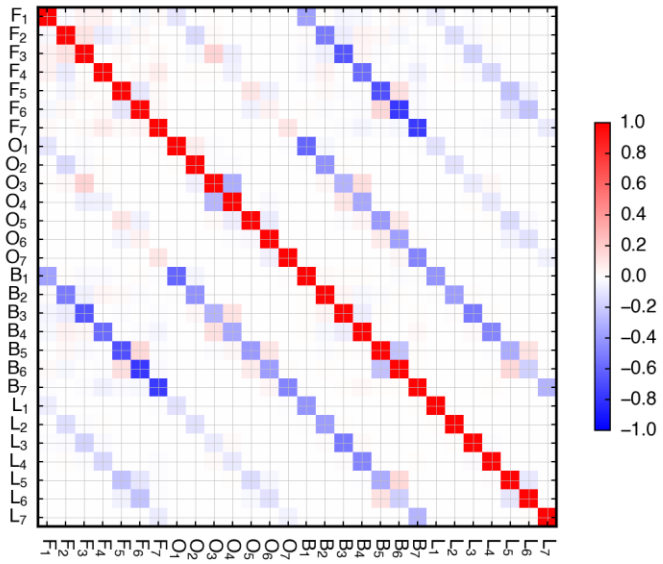

Table S1 Prior and posterior values and uncertainties (Pg C yr^{-1}). The adjusted O values (O_adj) from LQ15 that are not used in the optimization are also shown for a comparison with the unadjusted prior O values. The adjusted O values are on average 0.26±0.03 Pg C yr^{-1} smaller than the unadjusted ones.

		80-84	85-89	90-94	95-99	00-04	05-09	10-14
prior	F	5.27±0.28	5.79±0.41	6.18±0.35	6.55±0.35	7.19±0.39	8.40±0.53	9.16±0.41
	O	-1.70±0.50	-1.71±0.50	-1.98±0.50	-1.91±0.50	-1.98±0.50	-2.20±0.50	-2.43±0.50
	O_adj	-1.93±0.50	-1.94±0.50	-2.25±0.50	-2.15±0.50	-2.24±0.50	-2.48±0.50	-2.74±0.50
	B	-1.31±0.95	-1.89±0.83	-2.06±0.85	-2.08±0.80	-2.31±0.80	-2.43±0.80	-2.37±1.01
	L	1.30±0.62	1.39±0.65	1.78±0.94	1.83±1.04	1.20±0.70	0.94±0.65	1.00±0.70
posterior	F	5.22±0.27	5.77±0.38	5.96±0.31	6.43±0.32	7.17±0.33	8.03±0.40	9.14±0.37
	O	-1.82±0.40	-1.76±0.33	-2.02±0.19	-1.77±0.22	-2.45±0.24	-2.30±0.24	-2.69±0.26
	B	-1.86±0.53	-1.83±0.52	-3.07±0.45	-2.31±0.44	-1.64±0.42	-2.36±0.47	-2.82±0.50
	L	1.43±0.29	1.63±0.30	1.52±0.31	1.54±0.29	0.96±0.26	0.86±0.22	1.24±0.19
	B+L	-0.43±0.49	-0.20±0.49	-1.55±0.39	-0.77±0.40	-0.68±0.42	-1.50±0.48	-1.58±0.48

Table S2 Sources and values of different constraining data-streams used in the optimization. The blue and orange shades indicate the length of time covered. The constraining data tiers were defined as: Tier 1, direct carbon observations (e.g. CGR); Tier 2, indirect carbon observations unambiguously related to carbon quantities (e.g. O_2/N_2); Tier 3, direct carbon observations with an empirical (data-driven) model used to obtain global estimates, e.g. the use of geo-statistics to up-scale local data into global values; Tier 4, indirect carbon observations not simply related to global carbon flux quantities.

	80-84	85-89	90-94	95-99	00-04	05-09	10-14	Tier	Methods and References
CGR (Pg C yr^{-1})	2.94 ±0.22	3.81 ±0.22	2.35 ±0.18	3.89 ±0.18	3.93 ±0.16	4.12 ±0.16	4.80 ±0.16	1	The atmospheric CO_2 growth rate (CGR) is direct carbon observations from more than 60 monitoring stations from the NOAA/ESRL atmospheric network (14). Uncertainties are from "Table 1" in Ballantyne et al. (34), which are "the means of the decadal standard deviations". These uncertainties represent our ability to detect a change.
O_2/N_2 (per meg unit)			-6.10 ±0.22	-7.37 ±0.69	-8.89 ±0.30	-9.15 ±0.35	-10.64 ±0.37	2	Data are from Scripps O_2 program (http://scrippso2.ucsd.edu/), and the weighted average of data from stations of Alert, La Jolla and Cape Grim are taken as the global means as in Keeling et al. (15). The standard deviations across data from these stations are used as uncertainties. The Scripps O_2 program records changes in atmospheric oxygen levels by collecting air samples at monitoring stations over the world. The change of atmospheric O_2 is related to the change of net land flux (B+L) and fossil fuel emission (F) but it is insensitive the change of ocean flux (O). The relationship of $\Delta O_2 = -\alpha_F F + \alpha_B(B+L) + Z_{O2}$ from Keeling et al. (15) is used in this study. Here, only the growth rate of O2/N2 was used to constrain the sum of F and B+L here, in order not to duplicate the use of CGR.
O (Pg C yr^{-1})	-1.79 ±1.07	-1.85 ±1.07	-1.88 ±1.07	-1.53 ±1.07	-1.59 ±1.07	-2.02 ±1.07	-2.28 ±1.07	3	Values from Landschützer et al. (17) are added to an outgassing of 0.45 Pg C yr^{-1} and the corresponding uncertainties of outgassing (0.18 Pg C yr^{-1}) from Jacobson et al. (16). The estimates from Landschützer et al. (17) used a neural network approach primarily based on surface ocean pCO_2. Note that Landschützer et al. (17) used SOCATv2 data that starts in 1968, and there is data in their analysis for the 1980-1984 period although not much. Both Landschützer et al., (17) and Rödenbeck et al. (18) used pCO_2 data, but they conducted independent approaches to upscale flux and get very different regional results (see the Surface Ocean pCO_2 Mapping (SOCOM) intercomparison paper by Rödenbeck et al. (37)). In our inversion, we estimated the potential error correlations between these two O data sets from the series of annual fluxes of the two products by assuming that the correlation in annual fluxes within each 5-year period is an approximation of the 5-year mean flux error correlation. The temporal correlations between the uncertainties in different 5-year intervals for these two data sets were also estimated using the method from Ballantyne et al. (34). In addition, sensitivity tests using only one of these two O data sets were also performed.
O (Pg C yr^{-1})		-1.82 ±0.68	-2.03 ±0.68	-1.68 ±0.68	-1.76 ±0.68	-1.56 ±0.68	-2.39 ±0.68	3	Values from Rödenbeck et al. (18) are added to an outgassing of 0.45 Pg C yr^{-1} and the corresponding uncertainties of outgassing (0.18 Pg C yr^{-1}) from Jacobson et al. (16). Rödenbeck et al. (18) estimated the ocean carbon fluxes using a diagnostic mixed-layer approach based on surface pCO_2 observation and mass conservation. The uncertainty of estimate of Rödenbeck et al. (18) is calculated from in Rödenbeck et al. (38) by assuming that range of the sensitivity tests represents its 1-σ range. See above for the possible relationship with O estimates from Landschützer et al., (17).
O (Pg C yr^{-1})			-2.00 ±0.40					4	Means and uncertainties are from McNeil et al. (19) to constrain O from 1990 to 1999. This decadal O estimate is based on CFCs data. McNeil et al. (19) estimated O using CFC-12 data only. Khatiwala et al. (20) used CFC-12, CFC-11 and ^{14}C for surface-to-interior transit time, complemented by temperature, salinity, oxygen and phosphate to get information on end-member to determine the types of waters that are being mixed. The method of Khatiwala et al. (20) thus uses much more information although there is a little overlap. A sensitivity test without using data from McNeil et al. (19) was conducted, and the results are rather consistent.
O (Pg C yr^{-1})			-1.91 ±0.60	-2.05 ±0.60				4	Means and uncertainties are from Khatiwala et al. (20). These estimates were based on field measurements of oceanic tracers, such as chlorofluorocarbons (CFCs), natural ^{14}C, temperature and salinity from the GLODAP and World Ocean Atlas databases. See above for the possible relationship with O estimates from McNeil et al. (19).
O(Pg C yr^{-1})			-1.80 ±0.20					4	Means and uncertainties are from Steinkamp and Gruber (21) to constrain O from 1990 to 1999. This O estimate was

								derived from an atmosphere-ocean inversion using atmospheric CO_2, ocean interior dissolved inorganic carbon (DOC) and surface pCO_2 data, and inventory-based land fluxes. It should be noted they only used the mean CO_2 level in the atmosphere, not the CGR, and thus there is no double use of data. Although this estimate of O included atmospheric CO_2, but it only used the mean CO_2 level in the atmosphere rather than the variations of CGR used in this study. Thus, there is no correlation with CGR.
B (Pg C yr^{-1})				-2.05 ±1.09	-1.85 ±1.13		3	Means are from Pan et al. (22) and corrected for river outgassing fluxes (16). They estimated global forest carbon stock and fluxes using a bottom-up approach based on inventories and long-time field observations. Given that B here only accounts for the carbon sink in global established forests, the uncertainties of global residuals in "Table 3" from Pan et al. (22) are also included, which may represent the uncertainty of land carbon sinks from other ecosystems like grassland. No correlation with other data except for Africa. RECCAP used B estimate in Africa from Pan et al. (22), and we used the sum of regional net ecosystem exchange (NEE) from RECCAP to constrain B+L. But the contribution of NEE in Africa to the global NEE is very small (see Table S3), and thus the correlation between B from Pan et al. (22) and B+L from RECCAP was not included here.
B+L (Pg C yr^{-1})					-1.29 ±0.61		3	RECCAP (see Table S3). Net ecosystem exchange (NEE) from RECCAP are data-driven products estimated based on regional carbon cycle using various data sources (see Table S3). The B+L used here refers to the global (sum of regional values) anthropogenic NEE (corrected for river outgassing fluxes of 0.45 ±0.18 Pg C yr^{-1} from Jacobson et al.(16)) in Table S3. Potentially small correlation with B from Pan et al. (22) was ignored (see above).
L (Pg C yr^{-1})	1.33 ±0.50	1.52 ±0.50	1.56 ±0.50	1.64 ±0.50	1.04 ±0.50	0.87 ±0.50	0.88 ±0.50	3	Means and uncertainties are from the bookkeeping model by Houghton et al. (24), which is also used in the global carbon budget from Le Quéré et al. (8). The bookkeeping model from Houghton et al. (24) used inventory data from FAO to track the area of land use change, and combined carbon density in different carbon pools (e.g. vegetation and soil) to estimate the land use change fluxes. Although both Houghton et al. (24) and Hansis et al. (23) used bookkeeping methods, they used different land use change maps and included different processes. Houghton et al. (24) used FAO/FRA land use change data as input while Hansis et al. (23) used Land-Use Harmonization (LUH) data (39). Therefore, there is no error correlation between the two L estimates.
L (Pg C yr^{-1})	1.76 ±0.49	1.89 ±0.52	1.82 ±0.50	1.54 ±0.43	1.27 ±0.40	1.13 ±0.28	1.36 ±0.22	3	Means and uncertainties are from the BLUE model by Hansis et al. (23). BLUE model is a spatially explicit bookkeeping model and tracks histories of successive land use and land cover change and their interactions in each grid cell. It also accounts for the gross land use and land cover transitions rather than net ones. The uncertainties here refer to the difference with the alternative estimates using different carbon density. See above for possible relationship with L from Houghton et al. (24)

Table S3 The estimates of net ecosystem exchange (NEE) from Regional Carbon Cycle Assessment and Processes (RECCAP) international research project. In brief, the observed carbon fluxes in the nine regions were evaluated and summed to give the global fluxes. NEE is calculated from the mass balance of the change in territorial carbon stocks and the lateral carbon fluxes (soil carbon export to river, river outgassing to ocean, crop and wood export) in each region. The global NEE corrected for river outgassing flux (16) is used to constrain B+L in this study. Negative values indicate a flux from the atmosphere to the land.

region	flux	period	Mean (Tg C yr^{-1})	Uncertainty (Tg C yr^{-1})	References in the mass balance calculation
North America	NEE	2000-2009	-418	288	King et al. (40); Peters et al. (41)
Europe	NEE	2000-2007	-234	166	Luyssaert et al. (26); Peters et al. (41); Hartmann et al. (42)
Russia	NEE	2007-2009	-600	224	Dolman et al. (43); Hartmann et al. (42)
South Asia	NEE	2000-2009	-86	34	Liu et al. (28); Peters et al. (41); Hartmann et al. (42)
East Asia	NEE	2000-2009	-256	35	Piao et al. (25); Lauerwald et al. (44); Peters et al. (41); Hartmann et al. (42)
Southeast Asia	NEE	undefined	-97	186	Liu et al. (28); Peters et al. (41); Hartmann et al. (42)
South America	NEE	2000-2009	11	284	Gloor et al. (45); Peters et al. (41); Hartmann et al. (42)
Africa	NEE	2000-2007	12	292	Pan et al. (22); Valentini et al. (46); Peters et al. (41); Hartmann et al. (42)
Australia	NEE	1990-2011	-71	36	Haverd et al. (47); Hartmann et al. (42)
Globe	NEE	2000-2009	-1740	604	sum of regional NEE
	B+L	2000-2009	-1290	611	NEE corrected for river outgassing to ocean (16)